This article was downloaded by: *[CAS Chinese Academy of Sciences]*
On: *27 February 2011*
Access details: *Access Details: [subscription number 931694359]*
Publisher *Taylor & Francis*
Informa Ltd Registered in England and Wales Registered Number: 1072954 Registered office: Mortimer House, 37-41 Mortimer Street, London W1T 3JH, UK

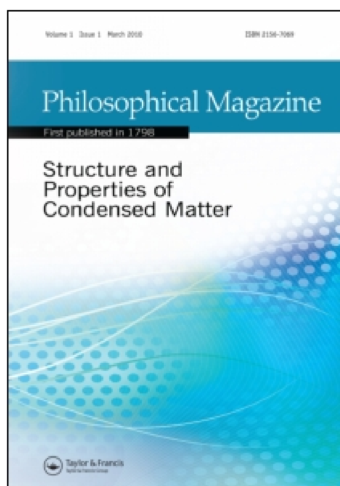

Philosophical Magazine
Publication details, including instructions for authors and subscription information:
http://www.informaworld.com/smpp/title~content=t713695589

Tensile strength of aluminium nitride films

Deng Gang Zong[a]; Chung Wo Ong[a]; Manju Aravind[a]; Mei Po Tsang[a]; Chung Loong Choy[a]; Deren Lu[b]; Dejun[a]
[a] Department of Applied Physics and Materials Research Centre, The Hong Kong Polytechnic University, Hung Hom, Kowloon, Hong Kong, PRC [b] State Key Laboratory of Transducer Technology, Shanghai Institute of Metallurgy, Academy of Sciences, Shanghai, China

To cite this Article Zong, Deng Gang , Ong, Chung Wo , Aravind, Manju , Tsang, Mei Po , Choy, Chung Loong , Lu, Deren and Dejun(2004) 'Tensile strength of aluminium nitride films', Philosophical Magazine, 84: 31, 3353 — 3373
To link to this Article: DOI: 10.1080/14786430412331283604
URL: http://dx.doi.org/10.1080/14786430412331283604

PLEASE SCROLL DOWN FOR ARTICLE

Full terms and conditions of use: http://www.informaworld.com/terms-and-conditions-of-access.pdf

This article may be used for research, teaching and private study purposes. Any substantial or systematic reproduction, re-distribution, re-selling, loan or sub-licensing, systematic supply or distribution in any form to anyone is expressly forbidden.

The publisher does not give any warranty express or implied or make any representation that the contents will be complete or accurate or up to date. The accuracy of any instructions, formulae and drug doses should be independently verified with primary sources. The publisher shall not be liable for any loss, actions, claims, proceedings, demand or costs or damages whatsoever or howsoever caused arising directly or indirectly in connection with or arising out of the use of this material.

PHILOSOPHICAL MAGAZINE, 1 NOVEMBER 2004
VOL. 84, NO. 31, 3353–3373

Taylor & Francis
Taylor & Francis Group

Tensile strength of aluminium nitride films

DENG GANG ZONG, CHUNG WO ONG†, MANJU ARAVIND, MEI PO TSANG, CHUNG LOONG CHOY, DEREN LU‡ and DEJUN MA

Department of Applied Physics and Materials Research Centre, The Hong Kong Polytechnic University, Hung Hom, Kowloon, Hong Kong, PRC
‡State Key Laboratory of Transducer Technology, Shanghai Institute of Metallurgy, Academy of Sciences, Shanghai, China

[*Received 4 June 2003 and accepted in revised form 27 May 2004*]

Downloaded By: [CAS Chinese Academy of Sciences] At: 08:01 27 February 2011

ABSTRACT

Two-layered aluminium nitride (AlN)/silicon nitride microbridges were fabricated for microbridge tests to evaluate the elastic modulus, residual stress and tensile strength of the AlN films. The silicon nitride layer was added to increase the robustness of the structure. In a microbridge test, load was applied to the centre of a microbridge and was gradually increased by a nano-indenter equipped with a wedge tip until the sample was broken, while displacement was recorded coherently. Measurements were performed on single-layered silicon nitride microbridges and two-layered AlN/silicon nitride microbridges respectively. The data were fitted to a theory to derive the elastic modulus, residual stress and tensile strength of the silicon nitride films and AlN films. For the AlN films, the three parameters were determined to be 200, 0.06 and 0.3 GPa, respectively. The values of elastic modulus obtained were consistent with those measured by conventional nano-indentation method. The tensile strength value can be used as a reference to reflect the maximum tolerable tensile stress of AlN films when they are used in micro-electromechanical devices.

§ 1. INTRODUCTION

Functional ceramic materials have been used in the development of microelectromechancial systems (MEMS). In a strategic report assessing the R&D work on MEMS (Committee on Advanced Materials and Fabrication Methods for Microelectromechancial Systems 1997), it was pointed out that stress-related failure of materials used to made MEMS would be a challenging issue in the future development of this field. Piezoelectric aluminium nitride (AlN) films find increasing applications in MEMS, particularly for actuation and sensing of mechanical vibrations. In a thin film bulk acoustic wave resonator (TFBAR), an AlN film is sandwiched between two metallic electrodes to give a resonance frequency exceeding 2 GHz and is proposed to be used in new generation mobile communication systems (Löbl *et al.* 2001, Dubois and Muralt 2002). AlN films can also be used in high temperature strain gauges (Gregory *et al.* 1996), force sensors, accelerometers and acoustic emission detectors (Zheng *et al.* 1993). All these devices are required to work in a vibrating environment. Moreover, to enhance the sensing and/or actuation performance of a device, AlN film is preferred to be deposited on some compliant

†Author for correspondence. Email: apacwong@inet.polyu.edu.hk.

Philosophical Magazine ISSN 1478–6435 print/ISSN 1478–6443 online © 2004 Taylor & Francis Ltd
http://www.tandf.co.uk/journals
DOI: 10.1080/14786430412331283604

parts, such as a membrane or a cantilever. An AlN film in a device would therefore face a risk of fracture, since AlN is a ceramic material and so would exhibit some degree of brittleness (Furuta and Uchino 1993, Lee and White 1998, Kusaka *et al.* 2002). Some methods are thus required for determining the film-only mechanical properties of a ceramic film. The fracture properties of a film are crucially important to reflect the conditions at which the film, and hence the whole device, will fail. To date, most experiments for measuring the fracture properties of thin films are conducted with the films adhered on substrates. The data from such measurements contain the contributions from both the film and substrate, while the film-only fracture properties are difficult to separate. Some experiments were designed to directly measure the properties of substrate-free film samples. For example, a uniaxial tensile test was carried out on a free-standing ceramic film to produce a stress–strain curve (Cardinale and Tustison 1992). A bulge test was performed by applying a fluid pressure on a ceramic membrane to induce deformation, from which a stress–strain curve of the film material can be derived (Vlassak and Nix 1992). However, handling of a fragile substrate-free ceramic film is not an easy task. The microbridge test is yet another distinctive method developed recently (Zhang *et al.* 2000, Su *et al.* 2002) to obtain the mechanical properties of a film. In this method a film material is made in the shape of a microbridge and gradually increasing load is applied to its centre to generate a load-displacement curve. By fitting the data to a theory, the tensile strength, internal stress and elastic modulus of the film material can be determined.

In this paper, we report the results of the measurements of the elastic modulus, internal stress and tensile strength of magnetron sputtered AlN films by using microbridge tests. The measurements were done in two steps, namely on a single-layered silicon nitride microbridge first and then on an AlN/silicon nitride double-layered microbridge. The elastic modulus, internal stress and tensile strength of the silicon nitride films were derived first, which were then substituted into the formulation for a double-layered specimen. The corresponding three parameters of the AlN layer were then derived. Moreover, the values of the elastic modulus of the two substances were measured by conventional nano-indentation method and compared with those obtained from the microbridge tests in order to give further justification of the validity of the microbridge method. The fracture toughness of the two film materials was estimated and discussed.

§2. Experimental methods

Two groups of microbridges were prepared, i.e. single-layered silicon microbridges and double-layered AlN/silicon nitride microbridges. Silicon nitride films were deposited on a two-side polished (100) silicon wafer by using low-pressure chemical vapour deposition (LPCVD) at 840°C and 170 mTorr. The reactant gas was an admixture of $SiCl_2H_2$ and NH_3, with their flow rates in the ratio of 6 : 1. The films were post-annealed at 1100°C in an N_2 ambient for 2 h. The film thickness determined by a scanning electron microscope (SEM) was found to be about 0.4 μm. Photolithography/dry etching processes were carried out to open windows on one side of the wafer. The exposed silicon wafer was etched using KOH solution at 80°C, such that only silicon nitride membranes were left behind. The membrane was dry etched to produce an array of silicon nitride microbridges with different dimensions (86–89 μm long, 14–21 μm wide). The design of the processes and the nature of (100) Si single-crystal wafer result in an angle of 54.74° between the wall of the underlying

Downloaded By: [CAS Chinese Academy of Sciences] At: 08:01 27 February 2011

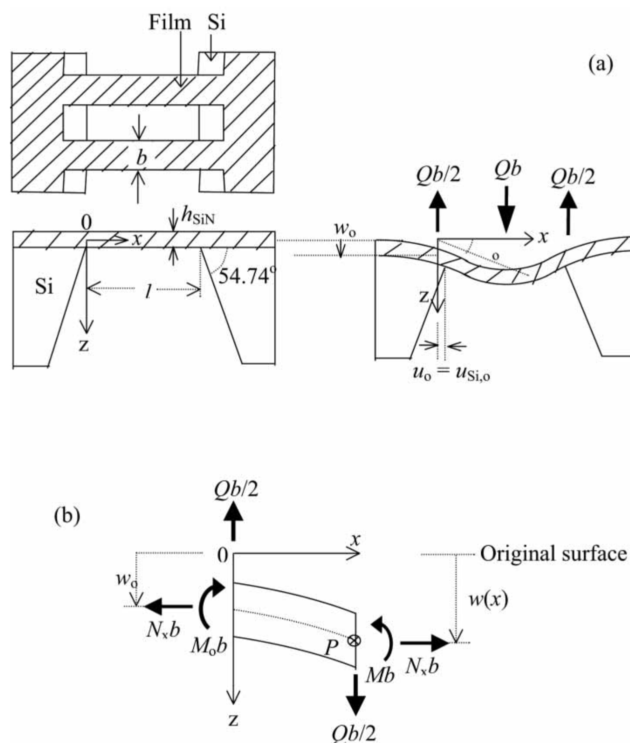

Figure 1. (*a*) Configuration of a single-layered silicon nitride microbridge and a schematic diagram showing the deformation of a microbridge subjected to a load. (*b*) Moments and forces acting on a segment.

Downloaded By: [CAS Chinese Academy of Sciences] At: 08:01 27 February 2011

silicon substrate and the film surface as depicted in figure 1. In addition, the microbridges were made to extend slightly into the supporting silicon substrate so as to prevent undercutting of the substrate.

Double-layered AlN/silicon microbridges were then produced by directly depositing AlN film onto the silicon nitride microbridges by using radio-frequency (RF) magnetron sputtering. The reactant gas was an admixture of argon and N_2 in a molar ratio of 1 : 1. The substrate temperature, ambient pressure and RF power during sputtering were 600°C, 5 mTorr and 180 W, respectively. A deposition run lasted for 3 hours. The lengths and widths of the double-layered microbridges varied in the ranges of 65–68 μm and 14–21 μm, respectively. The thickness of the AlN layer determined by SEM images was about 0.94 μm.

The microbridge tests were done using a nano-indenter (Nano Instruments Inc., Model IIs) equipped with a diamond wedge tip. The edge of the tip (30 μm) was wider than all the microbridge samples, and was aligned perpendicular to the length direction. Load was applied at the centre of a microbridge and was gradually increased. Displacement was recorded coherently until the sample was broken. In particular, the load was added in a constant-speed mode, where the wedge tip was controlled to proceed with a constant speed of $50\,\mathrm{nm\,s^{-1}}$ for a single-layered microbridge, and $20\,\mathrm{nm\,s^{-1}}$ for a double-layered microbridge. This configuration of experiments allowed a one-dimensional model to be used in the analysis, in which stresses were assumed to be unidirectional and along the length direction, while no lateral force was generated.

§ 3. Theory

3.1. *Single-layered silicon nitride microbridges*

The theory of bending of a single-layered microbridge is presented in this section. Figure 1(a) shows a single-layered silicon nitride microbridge, with the x-axis ($z=0$) coincident with the centre of the microbridge in the length direction, where h_{SiN}, l and b are, respectively, the thickness, length and width of the microbridge. When a load per unit width Q was applied at the centre position, $x=l/2$, the corresponding vertical displacement was (Appendix A) (Zhang *et al.* 2000, Su *et al.* 2002):

$$w(l/2)=-\frac{Q\tanh(kl/2)}{2N_{\mathrm{x}}k}+\frac{Ql}{4N_{\mathrm{x}}}-\frac{M_{\mathrm{o}}}{N_{\mathrm{x}}}\left[\frac{1}{\cosh(kl/2)}-1\right]+S_{\mathrm{PN}}(N_{\mathrm{x}}-N_{\mathrm{SiN}}^{\mathrm{r}})+S_{\mathrm{PP}}\frac{Q}{2}-S_{\mathrm{PM}}M_{\mathrm{o}} \quad (1)$$

In the equation, $k\equiv\sqrt{12N_{\mathrm{x}}/E_{\mathrm{SiN}}h_{\mathrm{SiN}}^{3}}$, where E_{SiN} is the elastic modulus of silicon nitride, and N_{x} the total force per unit width acting along the length. M_{o} is the bending moment per unit width acting on the cross-section at $x=0$. $N_{\mathrm{SiN}}^{\mathrm{r}}$ is the residual force per unit width acting on a cross-section.

Two simultaneous equations were established to correlate M_{o} and N_{x} (Appendix A). They are:

$$M_{\mathrm{o}}=\frac{S_{\mathrm{MN}}N_{\mathrm{x}}(N_{\mathrm{x}}-N_{\mathrm{SiN}}^{\mathrm{r}})+(S_{\mathrm{MP}}QN_{\mathrm{x}})/2+(Q)/2[(1/\cosh(kl/2))-1]}{S_{\mathrm{MM}}N_{\mathrm{x}}+k\tanh(kl/2)} \quad (2)$$

$$S_{\mathrm{NN}}(N_{\mathrm{x}}-N_{\mathrm{SiN}}^{\mathrm{r}})+S_{\mathrm{NP}}\frac{Q}{2}-S_{\mathrm{NM}}M_{\mathrm{o}}=\Theta-\frac{l(N_{\mathrm{x}}-N_{\mathrm{SiN}}^{\mathrm{r}})}{2E_{\mathrm{SiN}}h_{\mathrm{SiN}}} \quad (3)$$

The definition of Θ in equation (3) is:

$$\Theta=\frac{1}{8k}[(\chi^{2}+\xi^{2}+2\zeta^{2})kl+8(\chi-\xi)\zeta\sinh(kl/2)+2\chi\xi kl\cosh(kl)+(\chi^{2}+2\chi\xi-\xi^{2}+8\xi\zeta)\sinh(kl)+\xi^{2}\sinh(2kl)] \quad (4)$$

where

$$\chi=-\frac{Q\sinh(kl/2)+M_{\mathrm{o}}k}{N_{\mathrm{x}}\sinh(kl)} \quad (5)$$

$$\xi=\frac{M_{\mathrm{o}}k}{N_{\mathrm{x}}\sinh(kl)} \quad (6)$$

$$\zeta=\frac{Q}{2N_{\mathrm{x}}} \quad (7)$$

In these equations, the terms containing S_{ij} (i, j = N, P and M) have arisen from the deformability of the silicon substrate. With the values of S_{ij} as given in Appendix A, the elastic modulus and internal stress were evaluated by the following procedures. For a given load Q_{i}, trial values were assigned to E_{SiN} and $N_{\mathrm{SiN}}^{\mathrm{r}}$. They were substituted into equations (2) and (3), and the equations were solved numerically to obtain the solutions N_{xi} and M_{oi}. These values were then put into equation (1)

Downloaded By: [CAS Chinese Academy of Sciences] At: 08:01 27 February 2011

at corresponding load per unit width Q_i, so as to calculate the displacement $w(Q_i, E_{SiN}, N^r_{SiN})$. This calculation process was repeated at all the values of Q_i within the experimental range of load, to theoretically obtain the load-displacement curve. The deviation between the experimental $w_{exp}(Q_i)$ and theoretical curve was denoted by a quantity:

$$\text{Error} = \sum_i \left[w_{exp}(Q_i) - w(Q_i, E_{SiN}, N^r_{SiN})\right]^2 \tag{8}$$

Different trial values of E_{SiN} and N^r_{SiN} were set to minimise the value of "Error". The settings resulting in the best fit were denoted as E_{SiN^*} and $N^r_{SiN^*}$, which served as reasonable estimates to the elastic modulus and residual force per unit width of the film. The residual stress $\sigma^r_{SiN^*}$ was then calculated as $N^r_{SiN^*}/h_{SiN}$.

The largest tensile stress, in a microbridge being bent, was experienced at the centre of its lower surface. The tensile stress at this position before fracture should be equal to the tensile strength of the silicon nitride layer, and was denoted as $\sigma^{TenStren}_{SiN}$. The SEM image taken after fracture of a microbridge sample also supported this suggestion, since cracking was usually found to occur at a region near its centre. Hence the tensile strength of the single-layered silicon nitride film could be expressed as (Appendix A):

$$\sigma^{TenStren}_{SiN} = \frac{N_x}{h_{SiN}} - \frac{E_{SiN} h_{SiN}}{2} \frac{d^2 w}{dx^2}\bigg|_{x=l/2} \tag{9}$$

3.2. *Double-layered AlN/silicon nitride microbridges*

In this section, the formulation describing the bending of a double-layered microbridge is presented. Referring to figure 2, the x-axis ($z = 0$) lies along the central line in the length direction. With this co-ordinate system, the surfaces of the AlN layer and the silicon nitride layer were at $z = -z_2 \equiv -(h_{AlN} + h_{SiN})/2$, and $z = z_2$, respectively, where h_{AlN} was the thickness of the AlN layer. The interface between the two layers was at $z = z_1 \equiv (h_{AlN} - h_{SiN})/2$. When a load per unit width $\boldsymbol{Q}$ was applied to the centre of the microbridge ($x = l/2$), the vertical displacement was (Appendix B) expressed as (Su *et al.* 2002):

$$\begin{aligned} \boldsymbol{w}(l/2) = &-\frac{\boldsymbol{Q}\tanh(\boldsymbol{K}l/2)}{2\boldsymbol{N}_x\boldsymbol{K}} + \frac{\boldsymbol{Q}l}{4\boldsymbol{N}_x} - -\frac{\overline{\boldsymbol{M}}_o}{\boldsymbol{N}_x}\left[\frac{1}{\cosh(\boldsymbol{K}l/2)} - 1\right] \\ &+ \boldsymbol{S}_{PN}(\boldsymbol{N}_x - \boldsymbol{N}_r) + \boldsymbol{S}_{PP}\frac{\boldsymbol{Q}}{2} - \boldsymbol{S}_{PM}[\boldsymbol{M}_o - \boldsymbol{M}_r] \end{aligned} \tag{10}$$

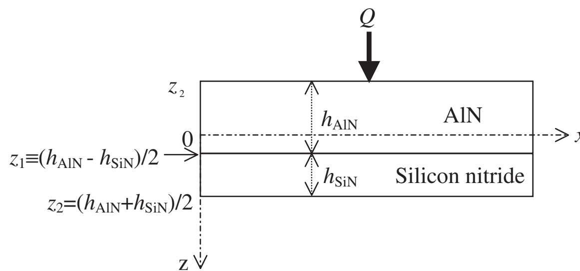

Figure 2. Double-layered AlN/silicon nitride microbridge.

Downloaded By: [CAS Chinese Academy of Sciences] At: 08:01 27 February 2011

In this equation, N_x is the total force per unit width in the length direction acting on a cross-section [figure 1(b)]. M_o is the bending moment per unit width acting on the cross-section at $x = 0$. We use the symbols σ^r_{AlN} and E_{AlN} to represent the residual stress and elastic modulus, respectively, of the AlN layer. Some of the quantities in equation (10) were defined as follows (Appendix B):

$$\begin{aligned}
\boldsymbol{K} &= \sqrt{\frac{\boldsymbol{N}_x}{\boldsymbol{B} - \boldsymbol{A}^2/\boldsymbol{D}}} \\
\boldsymbol{A} &= h_{SiN}h_{AlN}(E_{SiN^*} - E_{AlN})/2 \\
\boldsymbol{B} &= [E_{SiN^*}h_{SiN}(h^2_{SiN} + 3h^2_{AlN}) + E_{AlN}h_{AlN}(3h^2_{SiN} + h^2_{AlN})]/12 \\
\boldsymbol{D} &= E_{SiN^*}h_{SiN} + E_{AlN}h_{AlN} \\
\boldsymbol{M}_r &= \text{residual moment per width} = h_{SiN}h_{AlN}(\sigma^r_{SiN^*} - \sigma^r_{AlN})/2 \\
\boldsymbol{N}_r &= \text{residual force per width} = \sigma^r_{SiN^*}h_{SiN} + \sigma^r_{AlN}h_{AlN} \\
\overline{\boldsymbol{M}}_o &= \boldsymbol{M}_o - (\boldsymbol{N}_x - \boldsymbol{N}_r)\boldsymbol{A}/\boldsymbol{D} - \boldsymbol{M}_r
\end{aligned}$$

Two simultaneous equations relating M_o and N_x can be set up:

$$\begin{aligned}
&(\boldsymbol{M}_o - \boldsymbol{M}_r)[\boldsymbol{S}_{MM}\boldsymbol{N}_x + \boldsymbol{K}\tanh(\boldsymbol{K}l/2)] \\
&\quad = \boldsymbol{S}_{MN}\boldsymbol{N}_x(\boldsymbol{N}_x - \boldsymbol{N}_r) + \frac{\boldsymbol{S}_{MP}\boldsymbol{Q}\boldsymbol{N}_x}{2} + \frac{\boldsymbol{K}\boldsymbol{A}(\boldsymbol{N}_x - \boldsymbol{N}_r)}{\boldsymbol{D}}\tanh(\boldsymbol{K}l/2) + \frac{\boldsymbol{Q}}{2}\left[\frac{1}{\cosh(\boldsymbol{K}l/2)} - 1\right]
\end{aligned} \tag{11}$$

$$\begin{aligned}
&\boldsymbol{S}_{NN}(\boldsymbol{N}_x - \boldsymbol{N}_r) + \frac{\boldsymbol{S}_{NP}\boldsymbol{Q}}{2} - \boldsymbol{S}_{NM}(\boldsymbol{M}_o - \boldsymbol{M}_r) \\
&\quad = \Xi + \frac{\boldsymbol{A}}{\boldsymbol{D}}\left[\frac{\boldsymbol{Q}(\cosh(\boldsymbol{K}l/2) - 1)}{2\boldsymbol{N}_x\cosh(\boldsymbol{K}l/2)} + \overline{\boldsymbol{M}}_o\frac{\boldsymbol{K}}{\boldsymbol{N}_x}\tanh(\boldsymbol{K}l/2)\right] - \frac{l(\boldsymbol{N}_x - \boldsymbol{N}_r)}{2\boldsymbol{D}}
\end{aligned} \tag{12}$$

In equation (12), Ξ is defined as:

$$\Xi = \frac{\boldsymbol{Q}^2}{8\boldsymbol{K}\boldsymbol{N}_x^2}\left[\begin{array}{l}\left(\Lambda^2 + \Psi^2 + \frac{1}{2}\right)\boldsymbol{K}l + 4(\Lambda - \Psi)\sinh(\boldsymbol{K}l/2) + 2\Lambda\Psi\boldsymbol{K}l\cosh(\boldsymbol{K}l) \\ +(\Lambda^2 + 2\Lambda\Psi - \Psi^2 + 4\Psi)\sinh(\boldsymbol{K}l) + \Psi^2\sinh(2\boldsymbol{K}l)\end{array}\right]$$

$$\Lambda = -\frac{\sinh(\boldsymbol{K}l/2)}{\sinh(\boldsymbol{K}l)} - \frac{\overline{\boldsymbol{M}}_o\boldsymbol{K}}{\boldsymbol{Q}\sinh(\boldsymbol{K}l)}$$

$$\Psi = \frac{\overline{\boldsymbol{M}}_o\boldsymbol{K}}{\boldsymbol{Q}\sinh(\boldsymbol{K}l)}$$

The presence of the terms containing S_{ij} (i, j = P, M and N), i.e. the compliances of silicon, in the above equations were due to the deformability of the silicon substrate.

At a particular load per width Q_i, the analysis was started by assigning trial values to the elastic modulus E_{AlN} and internal stress σ^r_{AlN}, such that equations (11) and (12) could be solved numerically to give the solutions of M_o and N_x. The values of M_o and N_x, as well as Q_i, were used in equation (10) to calculate the displacement $w(Q_i, E_{AlN}, \sigma^r_{AlN})$. By varying Q_i to cover the experimental range of load, a theoretical load-displacement curve was obtained and was compared with the

Downloaded By: [CAS Chinese Academy of Sciences] At: 08:01 27 February 2011

experimental data $w_{\exp}$. The difference between the theoretically derived results and the experimental data was denoted by:

$$\mathbf{Error} = \sum_{i} [w_{\exp}(Q_i) - w(Q_i, E_{AlN}, \sigma^{r}_{AlN})]^2 \quad (13)$$

The value of "**Error**" was then minimized by assigning different trail values of E_{AlN} and σ^{r}_{AlN}. The optimized settings corresponding to the best fit were referred as E_{AlN^*} and $\sigma^{r}_{AlN^*}$, which respectively gave reasonable estimates for the elastic modulus and internal stress of the AlN film. Furthermore, the internal stresses at any points in the AlN and silicon nitride layers were:

$$\sigma_{AlN}(x, z) = E_{AlN^*}\left[\left(\frac{A}{D} - z\right)\frac{\partial^2 w}{\partial x^2} + \frac{N_x - N_r}{D}\right] + \sigma^{r}_{AlN^*} \quad (z = -z_2 \text{ and } z_1) \quad (14)$$

$$\sigma_{SiN}(x, z) = E_{SiN^*}\left[\left(\frac{A}{D} - z\right)\frac{\partial^2 w}{\partial x^2} + \frac{N_x - N_r}{D}\right] + \sigma^{r}_{SiN^*} \quad (z = z_1 \text{ and } z_2) \quad (15)$$

§4. Results and discussion

4.1. *Single-layered silicon nitride*

We first present the results of the tests on single-layered silicon nitride microbridges, which will be used in the next section for the analysis of the double-layered specimens. The upper curve of figure 3 (*a*) illustrates the typical load-displacement curve of a single-layered silicon nitride microbridge, and the best theoretical fitting (dotted line) to the data. The fracture point was indicated by an arrow, where a sudden drop in load accompanied by a drastic rise in the displacement was observed (not shown). The curve in the low-load range was magnified in figure 3 (*b*), showing that the fitting was quite acceptable. The results of the elastic modulus, internal stress and tensile strength of the silicon nitride film derived according to the theory of Section 3.1 for the microbridges of different widths are plotted in Figure 4 (*a*) to (*c*). The averages of the three groups of data were denoted respectively by $\langle E_{SiN^*}\rangle$, $\langle \sigma^{r}_{SiN^*}\rangle$ and $\langle \sigma^{TenStren}_{SiN}\rangle$, representing the final evaluation of the elastic modulus, internal stress and tensile strength of the silicon nitride film. Their numerical values are tabulated in table 1.

$\langle E_{SiN^*}\rangle$ was determined to be 270 ± 20 GPa. This value was compared with the result of elastic modulus of silicon nitride film measured using conventional nano-indentation tests with a 3-sided Berkovich diamond tip, in the presence of the substrate, as denoted by E^{indent}_{SiN}. In this method, the slope S of the unloading curve at the point of maximum load was extracted. The value of E^{indent}_{SiN} was assumed to be equal to $(2(1 - \nu^2)/S)\sqrt{A(h_c)/\pi}$, where $A(h_c)$ is the contact area at a contact depth of h_c corresponding to the maximum load and ν is the Poisson's ratio of the specimen, and was assumed to be 0.25 (Oliver and Pharr 1992). The data of E^{indent}_{SiN} are plotted against indentation depths in figure 5. A gradual drop of E^{indent}_{SiN} is observed when h_c exceeds $\approx$50 nm, because the indentation depths are larger than 1/10 of the thickness of the single-layered silicon nitride film (= 0.4 μm), so the deformation of the substrate is seriously enough to effect the measurements. The average of the data points (denoted as $\langle E^{indent}_{SiN}\rangle$) taken at h_c around 45 nm (i.e. 20–55 nm) was used as an estimate of E^{indent}_{SiN}, where the influence from the substrate was assumed to be

Downloaded By: [CAS Chinese Academy of Sciences] At: 08:01 27 February 2011

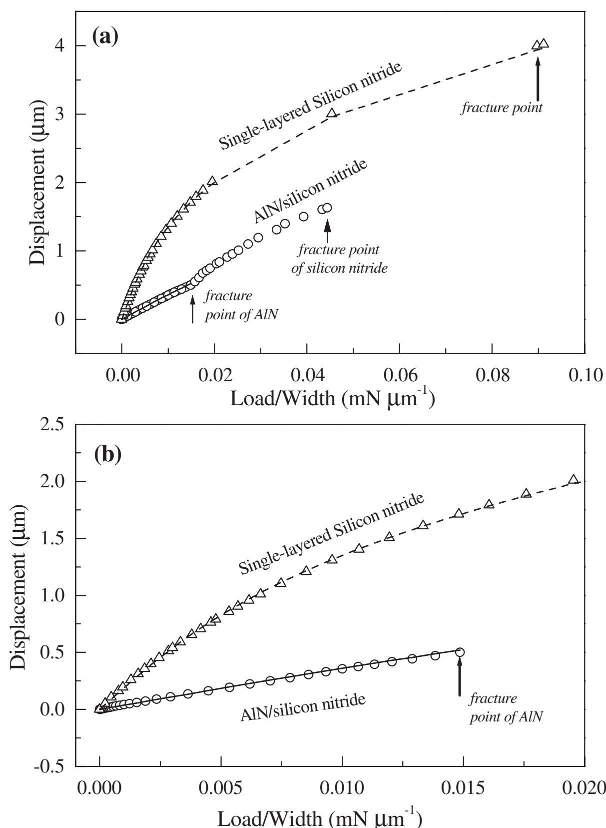

Figure 3. (*a*) Typical load-displacement curve of a single-layered silicon nitride microbridge (△) and a double-layered AlN/silicon nitride microbridge (○). Theoretical fittings to the data are also shown. (*b*) Exaggerated load-displacement curves at low load range.

Downloaded By: [CAS Chinese Academy of Sciences] At: 08:01 27 February 2011

negligibly small, though the data around this region are found to be more scattering. The value of $\langle E_{\rm SiN}^{\rm indent}\rangle$ is 250 ± 25 GPa, as shown in table 1. One immediately sees that $\langle E_{\rm SiN^*}\rangle$ and $\langle E_{\rm SiN}^{\rm indent}\rangle$ are fairly close, indicating that the results of the two methods are quite consistent. Moreover, $\langle E_{\rm SiN^*}\rangle$ was close to the elastic modulus of bulk stoichiometric Si_3N_4 (= 249 GPa), further supporting the validity of the microbridge method (Teter 1998).

All the data of $\sigma_{\rm SiN^*}^{\rm r}$ were positive [figure 4 (*b*)], indicating that the silicon nitride film was under tensile stress. The average of all the data, denoted as$\langle\sigma_{\rm SiN^*}^{\rm r}\rangle$, is 0.25 ± 0.05 GPa (table 1), which was an estimate of the internal stress in the film. Referring to the published data of the internal stress of silicon nitride films reported by different authors, one finds that the results are rather sensitive to the deposition techniques. For silicon nitride films prepared by LPCVD method, the internal stress is generally found to be tensile (0.29–1 GPa) (Adam 1985, Zhang *et al.* 2000). Our result of $\langle\sigma_{\rm SiN^*}^{\rm r}\rangle$ is quite acceptable, since it just lies slightly below this range.

The average value of the tensile strength [figure 4 (*c*)] determined from equation (9) was $\langle\sigma_{\rm SiN}^{\rm TenStren}\rangle = 4.9 \pm 0.5$ GPa. Published data for the tensile strength of silicon nitride are scattered within a broad range. For example, Cardinale and Tustison (1992) reported that the fracture strength of PECVD silicon nitride films was in the

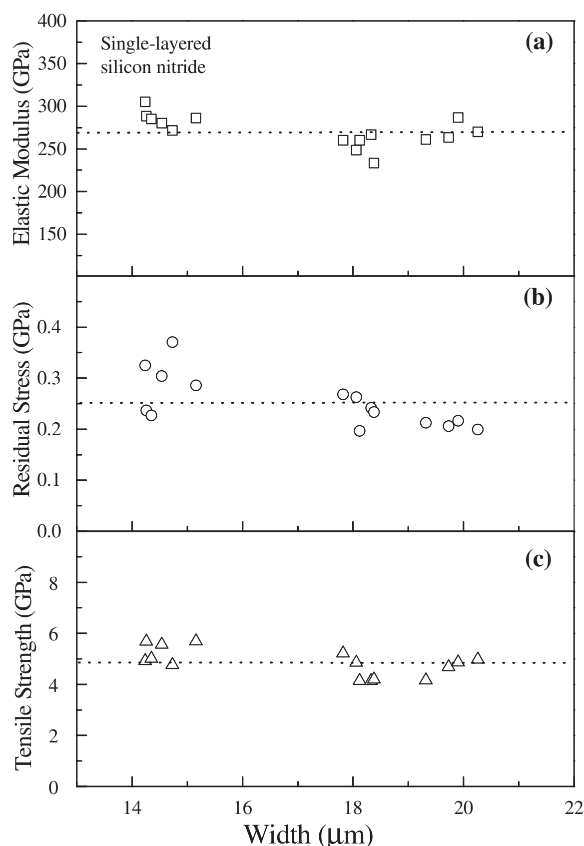

Figure 4. (*a*) Elastic modulus, (*b*) residual stress and (*c*) tensile strength of the silicon nitride films measured by microbridge tests on specimens of different widths (14 to 21 μm). $h_{\text{SiN}} = 0.4\,\mu\text{m}$.

Table 1. Mechanical properties of silicon nitride and AlN films determined by microbridge and nano-indentation tests.

Silicon nitride film	AlN film
$\langle E_{\text{SiN*}} \rangle = 270 \pm 20\,\text{GPa}$	$\langle E_{\text{AlN*}} \rangle = 200 \pm 60\,\text{GPa}$
$\langle E_{\text{SiN}}^{\text{indent}} \rangle = 250 \pm 25\,\text{GPa}$	$\langle E_{\text{AlN}}^{\text{indent}} \rangle = 240 \pm 25\,\text{GPa}$
$\langle \sigma_{\text{SiN*}}^{\text{r}} \rangle = 0.25 \pm 0.05\,\text{GPa}$	$\langle \sigma_{\text{AlN*}}^{\text{r}} \rangle = 0.06 \pm 0.05\,\text{GPa}$
$\langle \sigma_{\text{SiN}}^{\text{TenStren}} \rangle = 4.9 \pm 0.5\,\text{GPa}$	$\langle \sigma_{\text{AlN}}^{\text{TenStren}} \rangle = 0.3 \pm 0.06\,\text{GPa}$
$K_{\text{c,SiN}} = 1.7\,\text{MN}\,\text{m}^{-3/2}$	$K_{\text{c,AlN}} = 0.16\,\text{MN}\,\text{m}^{-3/2}$

range of 0.39–0.42 GPa according to the results of bulge tests. Budinski and Budinski (1999) quoted a flexural strength of 0.8 GPa for bulk silicon nitride. Yang and Paul (2002) reported a higher range of 10.8–11.7 GPa for LPCVD silicon nitride films based on bulge tests. Zhang *et al.* (2000) reported an even higher bending strength of 12.26 GPa for their LPCVD silicon nitride films by using microbridge tests. The measured value of the tensile strength $\langle \sigma_{\text{SiN}}^{\text{TenStren}} \rangle$ of our silicon nitride film is consistent with the above-mentioned ranges. In addition, according to an *ab initio*

Downloaded By: [CAS Chinese Academy of Sciences] At: 08:01 27 February 2011

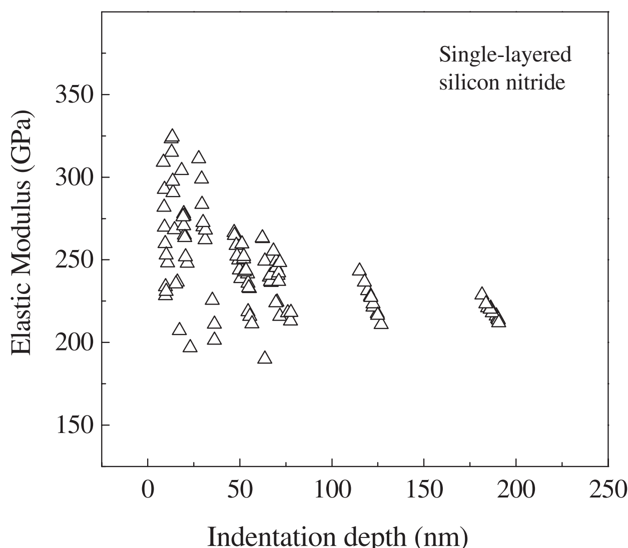

Figure 5. Elastic modulus of the silicon nitride films measured by nano-indentation tests using a 3-sided Berkovich diamond tip, with the films on substrates.

Downloaded By: [CAS Chinese Academy of Sciences] At: 08:01 27 February 2011

calculation, the strength of ideal beta-silicon nitride structure can reach the levels of 72.2 and 75 GPa, depending on whether the uni-axial tensile stress is applied along the [100] direction or [001] direction (Ogata *et al.* 2001). However, most of the values of the maximum tolerable tensile stress of silicon nitride measured experimentally are lower than the theoretically predicted values. This is because a ceramic material like silicon nitride would contain some microcracks, so that when it is under tensile stress, stresses would concentrate at the tips of microcracks, rendering the maximum tolerable tensile stress to be lower than the ideal levels (Cardinale and Tustison 1992).

4.2. *Double-layered AlN/silicon nitride*

After determining the mechanical properties of the silicon nitride film, we are ready to derive the mechanical properties of the AlN film. Figure 3 (*a*) shows the typical load-displacement curve of a double-layered AlN/silicon nitride microbridge. A solid curve passing through the data points in the low load range is the theoretical best fit. A kink was observed in the curve, which should be due to an initial cracking of the sample. More evidence (to be presented) showed that the cracking occurred at the surface of the AlN layer at $x = 0$. Meanwhile, the underlying silicon nitride layer was not damaged. Further increase in load eventually led to the fracture of the silicon nitride layer. This event can be identified by a sudden increase of displacement and rapid relaxation of load (not shown).

Figure 3 (*b*) shows the exaggeration of the load-displacement curve of the AlN/silicon nitride double-layered specimen in the low load range. The data of elastic modulus derived from this method for microbridges of different widths are plotted in figure 6 (*a*). The average of all the data, denoted as $\langle E_{\mathrm{AlN}^*} \rangle$, was calculated to be 200 ± 60 GPa as listed in table 1. Figure 7 shows a plot of elastic modulus data against indentation depths measured using nano-indentation tests. The thickness of the AlN film was about 0.94 μm. It is expected that for indentation depths

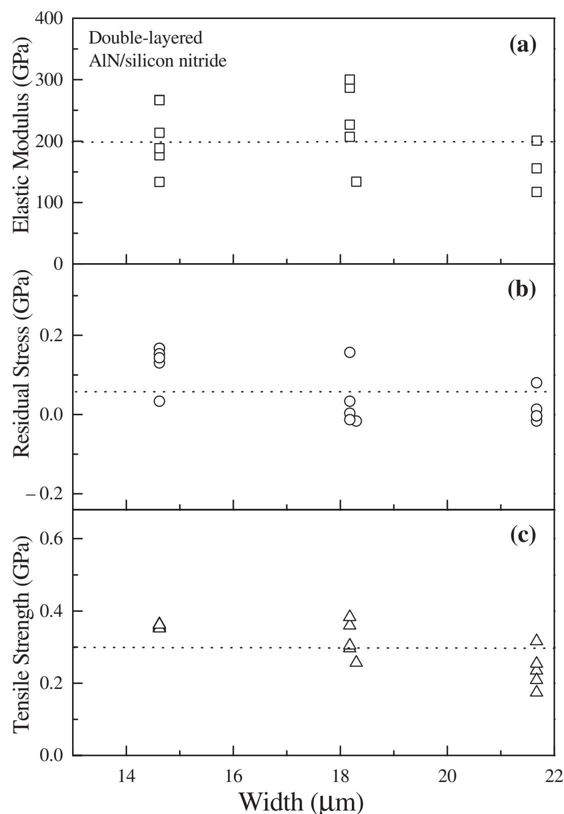

Figure 6. (*a*) Elastic modulus, (*b*) residual stress and (*c*) tensile strength of the AlN films calculated by microbridge tests on specimens having different widths (14 to 21 μm). $h_{AlN} = 0.9375\,\mu m$.

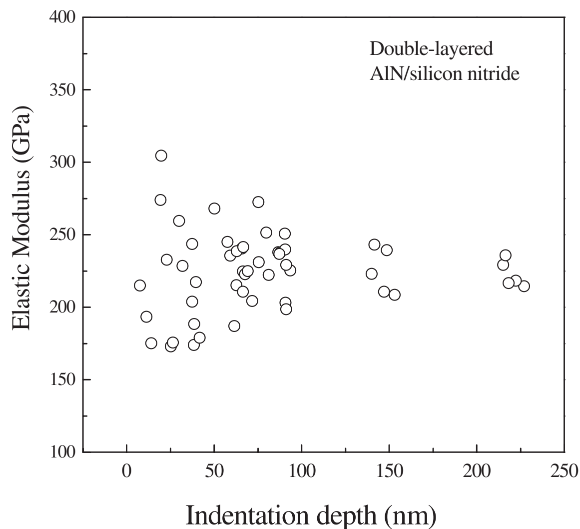

Figure 7. Elastic modulus of AlN films obtained by nano-indentation tests using a 3-sided Berkovich diamond tip, with the films on substrates.

Downloaded By: [CAS Chinese Academy of Sciences] At: 08:01 27 February 2011

below 220 nm as shown in figure 7, the influence due to substrate deformation is very little. The data points are seen to distribute round the same level, despite the presence of some scattering. The average of all the data measured at contact depths in the range of 25–100 nm was calculated to be $\langle E_{\mathrm{AlN}}^{\mathrm{indent}} \rangle = 240 \pm 25$ GPa (table 1), which is consistent with the $\langle E_{\mathrm{AlN}*} \rangle$ data. The validity of the microbridge method in determining the elastic modulus of the top layer of a doubled-layered microbridge structure is further verified. *Ab initio* calculations show that the elastic constant of hexagonal AlN crystal along the c-axis is 415 GPa (Ogata and Kitagawa 1999) and 373 GPa (Wright 1997). However, these high predicted values have not yet been observed experimentally. In fact, microcracks would exist in a polycrystalline ceramics, so that when the material is subjected to tensile forces, stresses would concentrate at the tips of microcracks. This effect lowers the maximum tolerable stress of a polycrystalline AlN film compared with the theoretically predicted value of an ideal AlN lattice.

The data of residual stresses for the AlN film obtained from the fitting are plotted in figure 6 (*b*). The values were positive, implying a tensile stress. The average of the data was $\langle \sigma_{\mathrm{AlN}*}^{\mathrm{r}} \rangle = 0.06 \pm 0.05$ GPa (table 1), giving an estimate of the internal stress in the AlN film. The reported values of the internal stress of AlN films prepared by magnetron sputtering are very sensitive to the ambient pressure during deposition. According to Kusaka *et al.* (2002) the internal stress in AlN films can change from compressive (−0.8 GPa) to tensile (0.7 GPa) when the ambient pressure is increased from 1 to 100 mTorr, where the lowest stress value appears at around 10 mTorr. The ambient pressure of 5 mTorr was employed in this study, and so the observation of a moderate internal stress is well understood.

Before discussing the results of the tensile strength of the AlN film, we need to interpret the kink as seen in the load-displacement curve of the double-layered microbridge as shown in figure 3 (*a*). Figure 8 shows the theoretical distributions of stresses along the length direction on the AlN surface, silicon nitride surface and the AlN/silicon nitride interface of a double-layered microbridge at the load of the kink. The stress on the AlN surface was calculated from equation (14) with $z = -z_2$. It shows a maximum tensile stress at $x/l = 0$, and then decreases with increasing x. The stress changes from being tensile to compressive at $x/l \approx 0.25$. The data in the range of $1/2 \leq x/l \leq 1$ were symmetric and not shown. On the other hand, the stress on the silicon nitride surface was obtained from equation (15) by setting $z = z_2$. The other two curves in figure 8 are the stresses as functions of x/l, generated on the AlN side and the silicon nitride side, respectively, at the AlN/SiN interface. They were calculated from equations (14) and (15), respectively, by setting $z = z_1$. One immediately finds from the figure that the tensile stresses in the silicon nitride layer do not exceed the tensile strength of the single-layered silicon nitride film $\langle \sigma_{\mathrm{SiN}}^{\mathrm{TenStren}} \rangle = 4.9$ GPa. Therefore, the occurrence of the kink could be attributed to the initial cracking of the upper surface of the AlN layer at $x = 0$, where the AlN layer experienced a maximum tensile stress. This theoretical prediction was confirmed by SEM images (inset, figure 8), which showed that specimens usually broke at one end of a microbridge. At the load of the kink as seen in figure 3 (*a*), the silicon nitride layer was not broken, until the load was increased to a level where a rapid rise in displacement and a sudden drop in load occurred. With this understanding, the tensile strength of the AlN layer was evaluated to be $\sigma_{\mathrm{AlN}}(0, -z_2)$, namely the stress on the upper surface of AlN film at the end of the microbridge, calculated at the load of the first kink observed in the load-displacement curve.

Downloaded By: [CAS Chinese Academy of Sciences] At: 08:01 27 February 2011

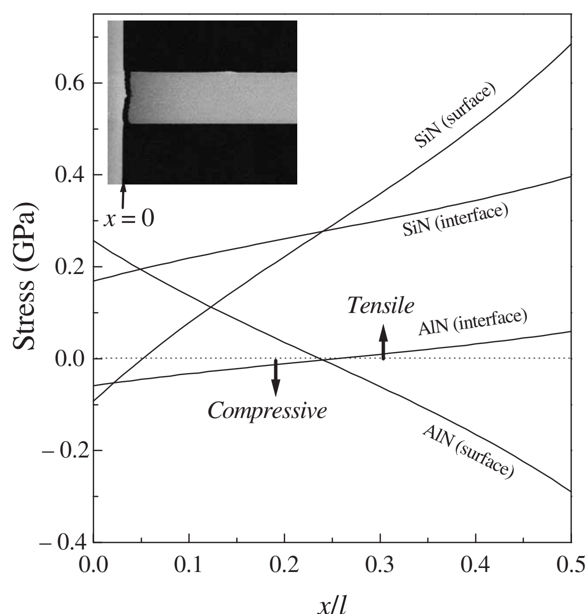

Figure 8. The calculated stress values at different positions along the length of an AlN/silicon nitride microbridge on the silicon nitride surface, AlN surface, and on the silicon nitride side and AlN side around the AlN/silicon nitride interface at a load where the AlN layer fractures. The inset is an SEM image of a fractured double-layered microbridge.

The tensile stresses of the AlN films of different widths extracted from individual calculations are plotted in figure 6(c). The average of all the data was $\langle\sigma_{\mathrm{AlN}}^{\mathrm{TenStren}}\rangle = 0.3 \pm 0.06$ GPa (table 1), which was believed to be a reasonable estimate of the tensile strength of the AlN film.

From the SEM images of the microbridges, it was seen that all the samples had regular geometric shape. The silicon nitride and AlN microbridges had widths in the range of 14–21 μm, and the lengths of the double-layered films were in the range of 65–69 μm. In particular, the variation in their width was typically of about 0.3%. Such a small variation in dimension is not expected to cause significant error to the measured mechanical properties. Figure 9 shows the maximum tensile stress values calculated in double-layered microbridges, of different lengths, under the load at the fracture point of the AlN layer. The data points represented by "○" show the tensile stress on the surface of the AlN film at $x = 0$, and the data points represented by "△" show the tensile stress on the lower surface of the silicon nitride film at $x = l/2$. From the scattering of the stress values in the figure we see that the measured mechanical properties of the films were not very sensitive to the length of the samples.

It was not easy to find published data for the tensile strength of AlN in thin film form to compare with our result. However, some data of the fracture strength of bulk AlN were available. The processing conditions will have an influence on the failure strength of AlN films. In a more recent study (Leung and Ong, in print), we showed that the structure of the magnetron sputtered AlN films could be either highly disordered, polycrystalline, textured, or epitaxial depending on the substrate

Downloaded By: [CAS Chinese Academy of Sciences] At: 08:01 27 February 2011

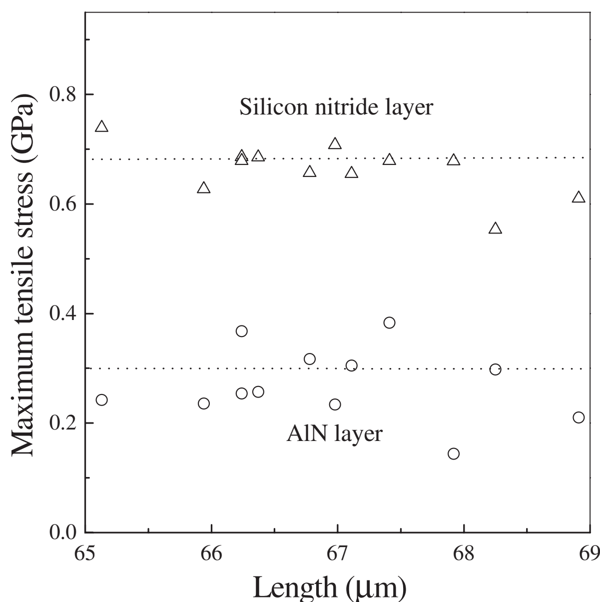

Figure 9. The calculated stress values on the AlN surface (○) at $x = 0$, and on the silicon nitride surface (△) at $x = l/2$ in double-layered microbridges of different lengths at the loads where fracture of the AlN layers occurred.

Downloaded By: [CAS Chinese Academy of Sciences] At: 08:01 27 February 2011

temperature, power of the radio-frequency (RF) radiation and the use of substrate materials. The features of defects, if any, were expected to be altered with the change in microstructure, which may lead to corresponding changes in the mechanical properties of the films. In the present study, the preparation conditions pertain to the production of polycrystalline AlN films. Hence the measured mechanical properties were due to the polycrystalline structure. In particular, the measured ultimate tolerable stresses would depend on the specific shape and distribution of the defects contained in the films and it might not be the same if the preparation conditions were changed. We further noted that Subhash and Ravichandran (1998) reported a flexural strength of 0.295 GPa for hot-pressed high purity AlN powder (Dow Chemical Co., MI) using four-point bending tests. Terao *et al.* (2002) claimed that AlN ceramics shows bending strengths of 0.353, 0.407 and 0.455 GPa after being doped with 5 mass% Y_2O_3, 5 mass% La_2O_3, and 5 mass% Sm_2O_3, respectively. The $\langle\sigma_{\rm AlN}^{\rm TenStren}\rangle$ value obtained in this study for AlN films is consistent with these values for bulk samples, and provides for the first time a reference value to reflect the maximum tolerable tensile stress of AlN in thin film form. The value is useful when using AlN film in MEMS device as it reflects the fracture properties which may affect the reliability of the device. Finally, compared with silicon nitride film, namely a widely used structural substance in devices, the maximum tolerable tensile stress of AlN film is 16 times weaker.

4.3. *Critical stress intensity factor*

It is known that the value of maximum tolerable tensile stress of a ceramic material is greatly affected by the presence of cracks, because stress concentration occurs at the tips of cracks. Irwin (Benham and Crawford 1987) defined a stress

intensify factor $K = \sigma(\pi a)^{1/2}$ to describe the elastic stress distribution near the crack tip, where σ is the externally applied stress and a is half the length of a crack. When σ reaches the maximum tolerable value, K is the critical stress intensity factor or fracture toughness (denoted as K_c). K_c depends on the elastic modulus and surface energy per unit area of a material, and so is related more closely to the fundamental properties of the material.

In the present study, we tried to use the measured $\langle\sigma_{SiN}^{TenStren}\rangle$ and $\langle\sigma_{AlN}^{TenStren}\rangle$ values to replace σ, in order to estimate the critical stress intensity factors (or fracture toughness, equal to the K value at the stress causing fracture) of the silicon nitride films and AlN films. They are denoted as $K_{c,SiN}$ and $K_{c,AlN}$. If the films were assumed to contain cracks with a size of 1/5 of the corresponding film thickness (i.e. 0.4 and 0.94 μm), which were aligned approximately along the thickness direction, $K_{c,SiN}$ and $K_{c,AlN}$ were estimated to be 1.4 and 0.16 MN m$^{-3/2}$, respectively (table 1). We notice that the former lies below the lower bound of the critical stress intensity factors of hot-pressed Si_3N_4 (3–10 MN m$^{-3/2}$) (Barsoum 1997).

Downloaded By: [CAS Chinese Academy of Sciences] At: 08:01 27 February 2011

§ 5. Conclusion

In this study we carried out microbridge tests on single-layered silicon nitride and double-layered AlN/silicon nitride microbridges to determine the mechanical properties, i.e. the elastic modulus, internal stresses and tensile strength, of substrate-free thin films. The most important goal was to determine the tensile strength of the AlN film, which was expected to be of great importance when utilising the film in the fabrication of devices.

In summary, the elastic modulus, internal stress and tensile strength of the silicon nitride film were determined to be 270 ± 20, 0.25 ± 0.05 and 4.9 ± 0.5 GPa, respectively. The result of the elastic modulus was consistent with that determined by using nano indentation tests (250 ± 25 GPa). The corresponding parameters of the AlN film were determined to be 200 ± 60, 0.06 ± 0.05 and 0.3 ± 0.06 GPa, respectively. The value of the elastic modulus thus measured by microbridge tests was consistent with the value determined by nano indentation tests (240 ± 25 GPa). The critical stress intensity factors of the two film materials were estimated to be $K_{c,SiN} = 1.7$ and $K_{c,AlN} = 0.16$ MN m$^{-3/2}$, by assuming that the films contained some microcracks with lengths of about 1/5 of the film thicknesses. By the present microbridge tests it was observed that the cracking of the structure as a result of applying a load was initiated on the upper surface of the AlN film on one end of the microbridge. The tensile strength of AlN film determined from this study was comparable to those reported for bulk AlN. Most importantly, our result for the first time provides a reference for the maximum tolerable tensile stress of an AlN film, the value of which must not be exceeded when the film material is used as the functional element in micro-sized devices.

Acknowledgements

This work was supported by the Centre for Smart Materials of the Hong Kong Polytechnic University (Code: 1.A.310), an internal grant of the Hong Kong Polytechnic University (Code: G-T 594), a Hong Kong ITF fund (Code: K.11.2A.ZP07), and Chinese National Project no. 1999033103.

APPENDIX A

Deformation of single-layered microbridges

The mission of this appendix is to establish the key equations (1)–(3) in the text for the analysis of the bending of a single-layered microbridge.

With the aid of figure 10, the displacement of a point at (x, z) along the x-direction $u_{\mathrm{SiN}}(x, z)$ is deduced from the theory of elastic deformation (Zhang *et al*. 2000, Su *et al*. 2002):

$$u_{\mathrm{SiN}}(x, z) = u_{\mathrm{SiN}}(x, 0) - z\frac{\partial w}{\partial x} \tag{A 1}$$

Referring to figure 11, the elongation of a line is $\triangle l = l - l_{\mathrm{o}}$, where l and l_{o} are expressed as (Zhang *et al*. 2000, Su *et al*. 2002):

$$l = \Delta x + u_{\mathrm{SiN}}(x + \Delta x, z + \Delta z) - u_{\mathrm{SiN}}(x, z)$$

$$l_{\mathrm{o}} = (\Delta x^2 + \Delta w^2)^{1/2} \approx \Delta x + \frac{1}{2}\left(\frac{\partial w}{\partial x}\right)^2 \Delta x$$

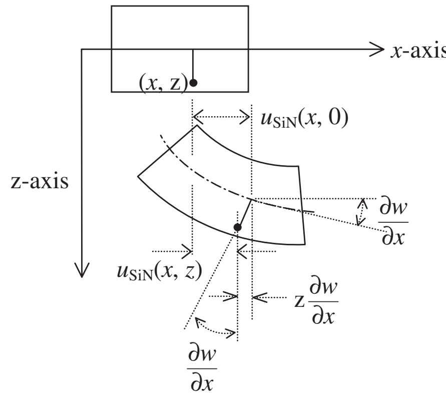

Figure 10. Displacement of a point at (x, z) due to the deformation of a single layered silicon nitride film. See equation (A 1).

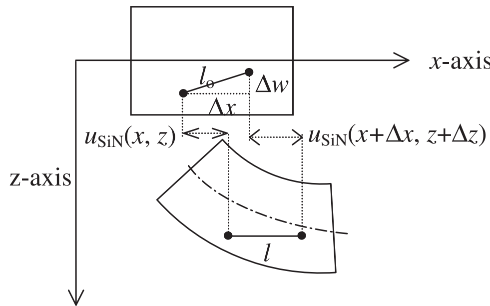

Figure 11. Strain along the x-direction due to the deformation of a single layered silicon nitride film. See equation (A 2).

Downloaded By: [CAS Chinese Academy of Sciences] At: 08:01 27 February 2011

The strain along the x-direction is thus derived to be:

$$\varepsilon_{\mathrm{SiN}} = \Delta l/l_{\mathrm{o}} = \frac{\partial u_{\mathrm{SiN}}(x,0)}{\partial x} + \frac{1}{2}\left(\frac{\partial w}{\partial x}\right)^2 - z\frac{\partial^2 w}{\partial x^2} \tag{A 2}$$

For simplicity, the symbol u_{SiN} is used to replace $u_{\mathrm{SiN}}(x, 0)$ hereafter. The expression of stress σ_{SiN} is written as:

$$\sigma_{\mathrm{SiN}} = E_{\mathrm{SiN}}\varepsilon_{\mathrm{SiN}} + \sigma^{\mathrm{r}}_{\mathrm{SiN}} = E_{\mathrm{SiN}}\left[\frac{\partial u_{\mathrm{SiN}}}{\partial x} + \frac{1}{2}\left(\frac{\partial w}{\partial x}\right)^2 - z\frac{\partial^2 w}{\partial x^2}\right] + \sigma^{\mathrm{r}}_{\mathrm{SiN}} \tag{A 3}$$

The bending moment per unit width (M), and the force per unit width in the x-direction (N_{x}) acting on a cross-section (Figure 1 (b)) are expressed as:

$$M = \int_{-t_{\mathrm{SiN}}/2}^{t_{\mathrm{SiN}}/2} \sigma_{\mathrm{SiN}} z \,\mathrm{d}z = -\frac{E_{\mathrm{SiN}} t^3_{\mathrm{SiN}}}{12}\frac{\partial^2 w}{\partial x^2} \tag{A 4}$$

$$N_{\mathrm{x}} = \int_{-t_{\mathrm{SiN}}/2}^{t_{\mathrm{SiN}}/2} \sigma_{\mathrm{SiN}} \,\mathrm{d}z = E_{\mathrm{SiN}}\frac{\partial u_{\mathrm{SiN}}}{\partial x} h_{\mathrm{SiN}} + \frac{1}{2}E_{\mathrm{SiN}}\left(\frac{\partial w}{\partial x}\right)^2 h_{\mathrm{SiN}} + N^{\mathrm{r}}_{\mathrm{SiN}} \tag{A 5}$$

A segment of a microbridge as shown in figure 1 (b) is in mechanical equilibrium, so that the total torque about a point P is zero:

$$-(w - w_{\mathrm{o}})N_{\mathrm{x}} + M_{\mathrm{o}}\frac{Q}{2}x - M = 0$$

By using the expression of M as shown in equation (A 4), the above equation becomes:

$$\frac{E_{\mathrm{SiN}} h^3_{\mathrm{SiN}}}{12}\frac{\partial^2 w}{\partial x^2} - N_{\mathrm{x}}(w - w_{\mathrm{o}}) + \frac{Q}{2}x + M_{\mathrm{o}} = 0, \quad (0 \le x \le l/2)$$

Defining $k \equiv \sqrt{N_{\mathrm{x}}/\left(E_{\mathrm{SiN}} h^3_{\mathrm{SiN}}/12\right)}$, this equation is rewritten as:

$$\frac{N_{\mathrm{x}}}{k^2}\frac{\partial^2 w}{\partial x^2} - N_{\mathrm{x}}(w - w_{\mathrm{o}}) + \frac{Q}{2}x + M_{\mathrm{o}} = 0 \quad (0 \le x \le l/2) \tag{A 6}$$

The general solution of a differential equation of this type is:

$$w(x,Q) = A'\cosh(kx) + B'\sinh(kx)\frac{Qx}{2N_{\mathrm{x}}} + \frac{M_{\mathrm{o}}}{N_{\mathrm{x}}} + w_{\mathrm{o}} \quad (0 \le x \le l/2)$$

From the boundary conditions $w(0,Q) = w_{\mathrm{o}}$, and $\partial w/\partial x\big|_{x=l/2} = 0$, the two constants are derived as $A' = -M_{\mathrm{o}}/N_{\mathrm{x}}$ and $B' = -(Q/kN_{\mathrm{x}})(\sinh(kl/2)/(\sinh(kl))-\left((M_{\mathrm{o}}/N_{\mathrm{x}})\left(1 - \cosh(kl)/\sinh(kl)\right)\right)$, respectively. The solution of w is:

$$w(x,Q) = -\frac{Q}{kN_x}\frac{\sinh(kl/2)}{\sinh(kl)}\sinh(kx) + \frac{Q}{2N_{\mathrm{x}}}x - \frac{M_{\mathrm{o}}}{N_{\mathrm{x}}}\left(\frac{\sinh(kx) + \sinh[k(l-x)]}{\sinh(kl)} - 1\right) + w_{\mathrm{o}} \tag{A 7}$$

Because of the deformability of the silicon substrate, the x- and z-direction displacements of the silicon substrate at $x = 0$ are not zero, and are denoted as $u_{\mathrm{Si,o}}$ and $w_{\mathrm{Si,o}}$. The angular deflection is $\theta_{\mathrm{Si,o}}$. They are related to the horizontal force per unit length $N_{\mathrm{x}} - N^{\mathrm{r}}_{\mathrm{Si}}$, the vertical force per unit length $Q/2$, and the torque per

Downloaded By: [CAS Chinese Academy of Sciences] At: 08:01 27 February 2011

unit length $-M_o$ through the compliances S_{ij} (i, j = N, P, M) of the silicon substrate [figure 1 (b)]:

$$\begin{bmatrix} u_{Si,o} \\ w_{Si,o} \\ \theta_{Si,o} \end{bmatrix} = \begin{bmatrix} S_{NN} & S_{NP} & S_{NM} \\ S_{PN} & S_{PP} & S_{PM} \\ S_{MN} & S_{MP} & S_{MM} \end{bmatrix} \begin{bmatrix} N_x - N_{Si}^r \\ Q/2 \\ -M_o \end{bmatrix} = \begin{bmatrix} u_o \\ w_o \\ \theta_o \end{bmatrix} \quad \text{(A 8)}$$

In the equation, u_o, w_o and θ_o are the x- and z-direction displacements, and angular deflection of the microbridge at its end ($x = 0$), and should be coherent with those of the silicon substrate. From finite element analysis (Su *et al.* 2002):

$$S_{NN} = 0.0545\,\mu m^2\,mN^{-1}, \qquad S_{PP} = 0.1373\,\mu m^2\,mN^{-1},$$

$$S_{MM} = 0.4173\,mN^{-1}, \qquad S_{NP} = S_{PN} = 0.0537\,\mu m^2\,mN^{-1},$$

$$S_{MN} = S_{NM} = 0.0113\,\mu m\,mN^{-1}, \quad S_{PM} = S_{MP} = 0.0367\,\mu m\,mN^{-1}$$

The second row of equation (A 8) is $w_o = w_{Si,o} = S_{PN}(N_x - N_{SiN}^r) + S_{PP}(Q/2) - S_{PM}M_o$. By substituting w_o in equation (A 7) and setting $x = l/2$, we get equation (1).

Equation (2) is obtained by differentiating equation (A 7):

$$\left.\frac{\partial w}{\partial x}\right|_{x=0} = \theta_o = \frac{Q[\cosh(kl/2) - 1]}{2N_x \cosh(kl/2)} + \frac{M_o k}{N_x}\tanh(kl/2) \quad \text{(A 9)}$$

and utilizing $\theta_o = \theta_{Si,o} = S_{MN}(N_x - N_{SiN}^r) + S_{MP}Q/2 - S_{MM}M_o$ according to the third row of equation (A 8).

To derive Equation (3), we start from integrating equation (A 5):

$$\int_0^{l/2} \frac{N_x - N_{SiN}^r}{E_{SiN}h_{SiN}} dx = \int_0^{l/2} \left[\frac{\partial u_{SiN}}{\partial x} + \frac{1}{2}\left(\frac{\partial w}{\partial x}\right)^2\right] dx$$

Due to symmetry, $u_{SiN}(x = l/2)$ is zero. From the above equation, the horizontal displacement of the microbridge at $x = 0$ is:

$$u_o = \frac{1}{2}\int_0^{l/2} \left(\frac{\partial w}{\partial x}\right)^2 dx - \frac{l}{2}\frac{N_x - N_{SiN}^r}{E_{SiN}h_{SiN}}$$

Replacing u_o by $S_{NN}(N_x - N_{SiN}^r) + S_{NP}Q/2 - S_{NM}M_o$ according to the first row of equation (A 8), one obtains:

$$S_{NN}(N_x - N_{SiN}^r) + S_{NP}\frac{Q}{2} - S_{NM}M_o = \frac{1}{2}\int_0^{l/2} \left(\frac{\partial w}{\partial x}\right)^2 dx - \frac{l}{2}\frac{N_x - N_{SiN}^r}{E_{SiN}h_{SiN}} \quad \text{(A 10)}$$

The expression of $\partial w/\partial x$ is obtained from equation (A 7), such that the integration $(1/2)\int_0^{l/2}(\partial w/\partial x)^2 dx$ can be carried out. This step will lead to equation (3). Meanwhile, the expressions of Θ and other related quantities defined by equations (4)–(7) appear naturally. Finally, the expression of $\sigma_{SiN}^{TenStren}$ in equation (10) is easily derived from equation (A 3) for σ_{SiN}.

Downloaded By: [CAS Chinese Academy of Sciences] At: 08:01 27 February 2011

APPENDIX B

Deformation of double-layered microbridges

The objective of this appendix is to show the steps for deriving the three key equations (10)–(12) for the study of a double-layered microbridge.

Analogous to (A 1), the displacements of a point in an AlN layer and a point in a silicon nitride layer of a double-layered structure along the x-direction are:

$$\begin{aligned} \boldsymbol{u}_{\mathrm{A1N}}(x,z) &= \boldsymbol{u}(x,0) - z\frac{\partial \boldsymbol{w}}{\partial x} \qquad (-z_2 \le z \le z_1, \text{ inside A1N}) \\ \boldsymbol{u}_{\mathrm{SiN}}(x,z) &= \boldsymbol{u}(x,0) - z\frac{\partial \boldsymbol{w}}{\partial x} \qquad (z_1 \le z \le z_2, \text{ inside silicon nitride}) \end{aligned} \tag{B 1}$$

Analogous to equation (A 2), it is proved that the strains in the x-direction are:

$$\begin{aligned} \boldsymbol{\varepsilon}_{\mathrm{A1N},x} &= \frac{\partial \boldsymbol{u}(x,0)}{\partial x} + \frac{1}{2}\left(\frac{\partial \boldsymbol{w}}{\partial x}\right)^2 - z\frac{\partial^2 \boldsymbol{w}}{\partial x^2} \qquad (-z_2 \le z \le z_1) \\ \boldsymbol{\varepsilon}_{\mathrm{SiN},x} &= \frac{\partial \boldsymbol{u}(x,0)}{\partial x} + \frac{1}{2}\left(\frac{\partial \boldsymbol{w}}{\partial x}\right)^2 - z\frac{\partial^2 \boldsymbol{w}}{\partial x^2} \qquad (z_1 \le z \le z_2) \end{aligned} \tag{B 2}$$

Replacing $\boldsymbol{u}(x, 0)$ by the symbol $\boldsymbol{u}$ for simplicity, the stresses are written as (notice the similarity with equation (A 3)):

$$\begin{aligned} \boldsymbol{\sigma}_{\mathrm{A1N}} &= E_{\mathrm{A1N}}\boldsymbol{\varepsilon}_{\mathrm{A1N}} + \sigma^{\mathrm{r}}_{\mathrm{A1N}} = E_{\mathrm{A1N}}\left[\frac{\partial \boldsymbol{u}}{\partial x} + \frac{1}{2}\left(\frac{\partial \boldsymbol{w}}{\partial x}\right)^2 - z\frac{\partial^2 \boldsymbol{w}}{\partial x^2}\right] + \sigma^{\mathrm{r}}_{\mathrm{A1N}} \quad (-z_2 \le z \le z_1) \\ \boldsymbol{\sigma}_{\mathrm{SiN}} &= E_{\mathrm{SiN}^*}\boldsymbol{\varepsilon}_{\mathrm{SiN},x} + \sigma^{\mathrm{r}}_{\mathrm{SiN}^*} = E_{\mathrm{SiN}^*}\left[\frac{\partial \boldsymbol{u}}{\partial x} + \frac{1}{2}\left(\frac{\partial \boldsymbol{w}}{\partial x}\right)^2 - z\frac{\partial^2 \boldsymbol{w}}{\partial x^2}\right] + \sigma^{\mathrm{r}}_{\mathrm{SiN}^*} \quad (z_1 \le z \le z_2) \end{aligned} \tag{B 3}$$

The bending moment per unit width and force per unit width acting on a cross-section of a microbridge are:

$$\boldsymbol{M} = \int_{-z_2}^{z_1} \boldsymbol{\sigma}_{\mathrm{AlN}} z\,\mathrm{d}z + \int_{z_1}^{z_2} \boldsymbol{\sigma}_{\mathrm{SiN}} z\,\mathrm{d}z = \boldsymbol{A}\left[\frac{\partial \boldsymbol{u}}{\partial x} + \frac{1}{2}\left(\frac{\partial \boldsymbol{w}}{\partial x}\right)^2\right] - \boldsymbol{B}\frac{\partial^2 \boldsymbol{w}}{\partial x^2} + \boldsymbol{M}_{\mathrm{r}} \tag{B 4}$$

$$\boldsymbol{N}_{\mathrm{x}} = \int_{-z_2}^{z_1} \boldsymbol{\sigma}_{\mathrm{AlN}}\,\mathrm{d}z + \int_{z_1}^{z_2} {}_{\mathrm{SiN}}\,\mathrm{d}z = \boldsymbol{D}\left[\frac{\partial \boldsymbol{u}}{\partial x} + \frac{1}{2}\left(\frac{\partial \boldsymbol{w}}{\partial x}\right)^2\right] - \boldsymbol{A}\frac{\partial^2 \boldsymbol{w}}{\partial x^2} + \boldsymbol{N}_{\mathrm{r}} \tag{B 5}$$

Considering the mechanical equilibrium of a segment of a microbridge, the total torque about a point (like P in figure 1 (b)) is zero:

$$-(\boldsymbol{w} - \boldsymbol{w}_{\mathrm{o}})\boldsymbol{N}_{\mathrm{x}} + \boldsymbol{M}_{\mathrm{o}} + \frac{\boldsymbol{Q}}{2}x - \boldsymbol{M} = 0 \tag{B 6}$$

Combining equation (B 4) and (B 5) to eliminate the term $\partial \boldsymbol{u}/\partial x + 1/2(\partial \boldsymbol{w}/\partial x)^2$, one obtains:

$$\boldsymbol{M} = \frac{\boldsymbol{A}}{\boldsymbol{D}}(\boldsymbol{N}_{\mathrm{x}} - \boldsymbol{N}_{\mathrm{r}}) + \left(\frac{\boldsymbol{A}^2}{\boldsymbol{D}} - \boldsymbol{B}\right)\frac{\partial^2 \boldsymbol{w}}{\partial x^2} + \boldsymbol{M}_{\mathrm{r}}$$

Downloaded By: [CAS Chinese Academy of Sciences] At: 08:01 27 February 2011

Putting this into equation (B 6) to remove $\boldsymbol{M}$, a differential equation is derived:

$$\left(\boldsymbol{B}-\frac{\boldsymbol{A}^2}{\boldsymbol{D}}\right)\frac{\partial^2 \boldsymbol{w}}{\partial x^2}-\boldsymbol{N}_{\mathrm{x}}(\boldsymbol{w}-\boldsymbol{w}_{\mathrm{o}})+\frac{\boldsymbol{Q}}{2}x+\left[\boldsymbol{M}_{\mathrm{o}}-\frac{\boldsymbol{A}}{\boldsymbol{D}}(\boldsymbol{N}_{\mathrm{x}}-\boldsymbol{N}_{\mathrm{r}})-\boldsymbol{M}_{\mathrm{r}}\right]=0$$

Defining $\overline{\boldsymbol{M}}_{\mathrm{o}} \equiv \boldsymbol{M}_{\mathrm{o}}-\frac{\boldsymbol{A}}{\boldsymbol{D}}(\boldsymbol{N}_{\mathrm{x}}-\boldsymbol{N}_{\mathrm{r}})-\boldsymbol{M}_{\mathrm{r}}$, this equation is rewritten as:

$$\left(\boldsymbol{B}-\frac{\boldsymbol{A}^2}{\boldsymbol{D}}\right)\frac{\partial^2 \boldsymbol{w}}{\partial x^2}-\boldsymbol{N}_{\mathrm{x}}(\boldsymbol{w}-\boldsymbol{w}_{\mathrm{o}})+\frac{\boldsymbol{Q}}{2}x+\overline{\boldsymbol{M}}_{\mathrm{o}}=0 \quad \text{or}$$
$$\frac{\boldsymbol{N}_{\mathrm{x}}}{\boldsymbol{K}^2}\frac{\partial^2 \boldsymbol{w}}{\partial x^2}-\boldsymbol{N}_{\mathrm{x}}(\boldsymbol{w}-\boldsymbol{w}_{\mathrm{o}})+\frac{\boldsymbol{Q}}{2}x+\overline{\boldsymbol{M}}_{\mathrm{o}}=0 \tag{B 7}$$

This equation has the same structure as that of equation (A 6), so that they have the solution like equation (A 7):

$$\boldsymbol{w}(x)=-\frac{\boldsymbol{Q}\sinh(\boldsymbol{K}l/2)}{\boldsymbol{N}_{\mathrm{x}}\boldsymbol{K}\sinh(\boldsymbol{K}l)}\sinh(\boldsymbol{K}x)$$
$$+\frac{\boldsymbol{Q}}{2\boldsymbol{N}_{\mathrm{x}}}x-\frac{\overline{\boldsymbol{M}}_{\mathrm{o}}}{\boldsymbol{N}_{\mathrm{x}}}\left[\frac{\sinh(\boldsymbol{K}x)+\sinh[\boldsymbol{K}(l-x)]}{\sinh(\boldsymbol{K}l)}-1\right]+\boldsymbol{w}_0 \quad (0\le x\le l/2) \tag{B 8}$$

Since the silicon substrate is deformable, the x- and z-direction displacements, and the angular deflection $\boldsymbol{\theta}_{\mathrm{Si,o}}$ of the silicon of the substrate at $x=0$ are related to the horizontal force per unit width $\boldsymbol{N}_{\mathrm{x}}-\boldsymbol{N}_{\mathrm{r}}$, vertical force per unit width $\boldsymbol{Q}/2$ and torque per unit width $-(\boldsymbol{M}_{\mathrm{o}}-\boldsymbol{M}_{\mathrm{r}})$ through the compliances of the silicon substrate $\boldsymbol{S}_{\mathrm{ij}}$ (i, j = P, M, N):

$$\begin{bmatrix}\boldsymbol{u}_{\mathrm{Si,o}}\\ \boldsymbol{w}_{\mathrm{Si,o}}\\ \boldsymbol{\theta}_{\mathrm{Si,o}}\end{bmatrix}=\begin{bmatrix}\boldsymbol{S}_{\mathrm{NN}} & \boldsymbol{S}_{\mathrm{NP}} & \boldsymbol{S}_{\mathrm{NM}}\\ \boldsymbol{S}_{\mathrm{PN}} & \boldsymbol{S}_{\mathrm{PP}} & \boldsymbol{S}_{\mathrm{PM}}\\ \boldsymbol{S}_{\mathrm{MN}} & \boldsymbol{S}_{\mathrm{MP}} & \boldsymbol{S}_{\mathrm{MM}}\end{bmatrix}\begin{bmatrix}\boldsymbol{N}_{\mathrm{x}}-\boldsymbol{N}_{\mathrm{r}}\\ \boldsymbol{Q}/2\\ -(\boldsymbol{M}_{\mathrm{o}}-\boldsymbol{M}_{\mathrm{r}})\end{bmatrix}=\begin{bmatrix}\boldsymbol{u}_{\mathrm{o}}\\ \boldsymbol{w}_{\mathrm{o}}\\ \boldsymbol{\theta}_{\mathrm{o}}\end{bmatrix} \tag{B 9}$$

The second equality states that the movement of the silicon substrate at $x=0$ is the same as that of the microbridge at the same point. According to finite element analysis (Su *et al.* 2002), the values of $\boldsymbol{S}_{\mathrm{ij}}$ are suggested to be:

$$\boldsymbol{S}_{\mathrm{NN}}=0.0545\,\mu\mathrm{m}^2\,\mathrm{mN}^{-1}, \qquad \boldsymbol{S}_{\mathrm{PP}}=0.106\,\mu\mathrm{m}^2\,\mathrm{mN}^{-1},$$
$$\boldsymbol{S}_{\mathrm{MM}}=0.0351\,\mathrm{mN}^{-1}, \qquad \boldsymbol{S}_{\mathrm{NP}}=\boldsymbol{S}_{\mathrm{PN}}=0.0361\,\mu\mathrm{m}^2\mathrm{mN}^{-1},$$
$$\boldsymbol{S}_{\mathrm{MN}}=\boldsymbol{S}_{\mathrm{NM}}=0.00495\,\mu\mathrm{m}\,\mathrm{mN}^{-1}, \quad \boldsymbol{S}_{\mathrm{PM}}=\boldsymbol{S}_{\mathrm{MP}}=0.0211\,\mu\mathrm{m}\,\mathrm{mN}^{-1}$$

Next, $\boldsymbol{w}_{\mathrm{o}}$ in equation (B 8) is replaced by the second row of equation (B 9), i.e. $\boldsymbol{S}_{\mathrm{PN}}(\boldsymbol{N}_{\mathrm{x}}-\boldsymbol{N}_{\mathrm{r}})+\boldsymbol{S}_{\mathrm{PP}}(\boldsymbol{Q}/2)-\boldsymbol{S}_{\mathrm{PM}}(\boldsymbol{M}_{\mathrm{o}}-\boldsymbol{M}_{\mathrm{r}})$. This leads to equation (10) in the text.

Equation (11) can be derived by differentiating equation (B 8) to give:

$$\left.\frac{\partial \boldsymbol{w}}{\partial x}\right|_{x=0}=\boldsymbol{\theta}_{\mathrm{o}}=\frac{\boldsymbol{Q}[\cosh(\boldsymbol{K}l/2)-1]}{2\boldsymbol{N}_{\mathrm{x}}\cosh(\boldsymbol{K}l/2)}+\frac{\overline{\boldsymbol{M}}_{\mathrm{o}}\boldsymbol{K}}{\boldsymbol{N}_{\mathrm{x}}}\tanh(\boldsymbol{K}l/2) \tag{B 10}$$

followed by a substitution $\boldsymbol{\theta}_{\mathrm{o}}$ by the third row of equation (B 9).

To derive equation (12), we start from integrating expression (B 5):

$$\int_0^{l/2}\frac{\boldsymbol{N}_{\mathrm{x}}-\boldsymbol{N}_{\mathrm{r}}}{\boldsymbol{D}}\mathrm{d}x=\int_0^{l/2}\left[\frac{\partial \boldsymbol{u}}{\partial x}+\frac{1}{2}\left(\frac{\partial \boldsymbol{w}}{\partial x}\right)^2-\frac{\boldsymbol{A}}{\boldsymbol{D}}\frac{\partial^2 \boldsymbol{w}}{\partial x^2}\right]\mathrm{d}x$$

Downloaded By: [CAS Chinese Academy of Sciences] At: 08:01 27 February 2011

Since $\boldsymbol{u}(x = l/2) = 0$, and $\partial \boldsymbol{w}/\partial x\big|_{x=l/2} = 0$, this expression becomes:

$$\boldsymbol{u}_{\mathrm{o}} = \frac{1}{2}\int_0^{l/2}\left(\frac{\partial \boldsymbol{w}}{\partial x}\right)^2 \mathrm{d}x + \frac{\boldsymbol{A}}{\boldsymbol{D}}\boldsymbol{\theta}_{\mathrm{o}} - \frac{l(\boldsymbol{N}_{\mathrm{x}} - \boldsymbol{N}_{\mathrm{r}})}{2\boldsymbol{D}} \tag{B 11}$$

$\boldsymbol{u}_{\mathrm{o}}$ is then replaced by the first row of equation (B 9), i.e. $\boldsymbol{u}_{\mathrm{Si,o}} = \boldsymbol{S}_{\mathrm{NN}}(\boldsymbol{N}_{\mathrm{x}} - \boldsymbol{N}_{\mathrm{r}}) + \boldsymbol{S}_{\mathrm{NP}}\boldsymbol{Q}/2 - \boldsymbol{S}_{\mathrm{NM}}(\boldsymbol{M}_{\mathrm{o}} - \boldsymbol{M}_{\mathrm{r}})$. In addition, the expression of $\partial \boldsymbol{w}/\partial x$ is derived from equation (B 8) and put into equation (B 11). On carrying out the integration $(1/2)\int_0^{l/2}(\partial \boldsymbol{w}/\partial x)^2 \mathrm{d}x$, equation (12) is obtained. The expressions of Ξ, Λ and Ψ follow naturally.

Finally, equations (14) and (15) for the internal stresses of the AlN and SiN layers are obtained by eliminating the term $\partial \boldsymbol{u}/\partial x + (1/2)(\partial \boldsymbol{w}/\partial x)^2$ from equations (B 3), with the aid of equation (B 5).

Downloaded By: [CAS Chinese Academy of Sciences] At: 08:01 27 February 2011

References

Adam, A. C., 1985, *VLSI Technology,* edited by S. M. Sze (Singapore: McGraw-Hill), p. 121.

Barsoum, M. W., 1997, *Fundamentals of Ceramics* (New York: McGraw-Hill), p. 401.

Benham, P. P., and Crawford, R. J., 1987, *Mechanics of Engineering Materials* (Singapore: Longman Scientific & Technical), p. 513.

Budinski, K. G., and Budinski, M. K., 1999, *Engineering Materials: Properties and Selection* (New Jersey: Prentice Hall), p. 694.

Cardinale, G. F., and Tustison, R. W., 1992, *Thin Solid Films*, **207**, 126.

Committee on Advanced Materials and Fabrication Methods for Microelectromechancial Systems, 1997, *Microelectromechanical Systems: Advanced Materials and Fabrication Methods* (Washington, DC: National Academy Press), p. 34.

Dubois, M. A., and Muralt, P., 2002, *Appl. Phys. Lett.*, **74**, 3032.

Furuta, A., and Uchino, K., 1993, *J. Am. Ceram. Soc.*, **76**, 1615.

Gregory, O .J., Slot, A. B., Amons, P.S., and Crisman, E. E., 1996, *Surf. Coatings Technol.*, **88**, 79.

Kusaka, K., Taniguchi, D., Hanabusa, T., and Tominaga, K., 2002, *Vacuum*, **66**, 441.

Lee, S. S., and White, R. M., 1998, *J. Micromech. Microengng*, **8**, 230.

Leung, T. T., and Ong, C. W., 2004, *Diamond Relat. Mater.*, **13**, 1603.

Löbl, H. P., Klee, M., Milsom, R., Dekker, R., Metzmacher, C., Bramd, W., and Lok, P., 2001, *J. Eur. Ceram. Soc.*, **21**, 2633.

Ogata, S., and Kitagawa, H., 1999, *Comput. Mater. Sci.*, **15**, 435.

Ogata, S., Hirosaki, N., Kocer, C., and Kitagawa, H., 2001, *Phys. Rev.* B, **64**, art. 172102.

Oliver, W. C., and Pharr, G. M., 1992, *J. Mater. Res.*, **7**, 1564.

Su, Y.-J., Qian, C.-F., Zhao, M.-H., and Zhang, T.-Y., 2002, *Acta mater.*, **48**, 4901.

Subhash, G., and Ravichandran, G., 1998, *J. Mater. Sci.*, **33**, 1933.

Terao, R., Tatami, J., Meguro, T., and Komeya, K., 2002, *J. Eur. Ceram. Soc.*, **22**, 1051.

Teter, D. M., 1998, *MRS Bull.*, **23**, 22.

Vlassak, J. J., and Nix, W. D., 1992, *J. Mater. Res.*, **7**, 3242.

Wright, A. F., 1997, *J. Appl. Phys.*, **82**, 2833.

Yang, J. L., and Paul, O., 2002, *Sensors Actuators* A, **97-98**, 520.

Zhang, T.-Y., Su, Y.-J., Qian, C.-F., Zhao, M.-H., and Chen, L.-Q., 2000, *Acta mater.*, **48**, 2843.

Zheng, L., Ramalingam, S., Shi, T., and Peterson, R. L., 1993, *J. Vac. Sci. Technol.* A, **11**, 2437.